A Robotic Control System for a Drill Jumbo with One Articulated Arm: Full-Scale Testing ⋆

Jonas Tønnessen [*,**] **Jan Tommy Gravdahl** [*]
Kristin Ytterstad Pettersen [*]

[*] *Department of Engineering Cybernetics, NTNU, O. S. Bragstads Plass 2D, 7034 Trondheim, Norway.*
[**] *Andersen Mek. Verksted AS (AMV), Svegeskogen 2, 4400 Flekkefjord, Norway.*

Abstract: This paper presents a robotic control system for an industrial drill jumbo with one articulated arm, developed for the AMV ZETA X boom, aiming to enhance the accuracy, efficiency, and safety of drill-and-blast tunneling operations. The system combines a Product-of-Exponentials forward kinematics model with a Newton-Raphson numerical inverse kinematics solver to compute joint configurations for a 6-DOF manipulator. Time-optimal joint trajectories are generated using ROS2/MoveIt2, and are tracked by PID controllers acting on the hydraulic actuators. The seventh joint, a feeder telescope, is controlled separately to establish and maintain contact with the rock face during drilling. The complete control algorithm autonomously executes a given digital drill plan, moving the 7-DOF manipulator from the current blast hole to the next and drilling each hole to its specified depth. The control system was experimentally validated in full-scale tests in Flekkefjord, Norway, and the Trælen mine, Norway, where multiple blast holes were drilled autonomously, achieving an average drilled hole accuracy of 4.6 cm and 19.1 cm, respectively. These results represent the first full-scale demonstration of numerical inverse-kinematics-based automatic control for drill jumbos and demonstrate the feasibility of the approach, marking an important step toward fully autonomous underground drilling rigs.

Keywords: Robotics, Tunnels and mines, Control systems, Kinematics, Motion Control

1. INTRODUCTION

1.1 Motivation

The increased global demand for raw materials, coupled with the depletion of shallow mineral deposits, forces exploitation of raw materials at greater depths (Wagner, 2019). This promotes autonomous and remote-controlled operations. Exploitation at greater depths introduces demanding operating conditions, primarily elevated rock stress and higher ambient temperatures.

The implementation of autonomous solutions in the drilling operation may also significantly increase both accuracy and efficiency. According to Mancini et al. (1996), drilling accuracy is the most important factor influencing the quality and cost of tunneling. Two metrics determine the quality of a blast round: advancement efficiency and overbreak. The former is defined as the ratio of the actual advance per blast round to the designed advance. The latter is the average thickness of rock removed beyond the designed tunnel profile. Mancini et al. (1996) compared direct manual joint control with automatic computerized control. The results indicate that automatic control can reduce overbreak by a factor of three and increase the advancement efficiency by five percentage points compared to manual control.

In addition to accuracy, the cycle time required to drill a full blast round is crucial for reducing cost. This duration is influenced by the time required to move the manipulator between holes and by whether the drill plan is executed in an optimal sequence. Li et al. (2023) presents an algorithm capable of reducing the travel distance of the manipulator when executing an entire drill plan by 35% compared to traditional traversal methods.

The conventional operation of the drill jumbo in Figure 1 is based on manual control. By introducing a robotic control system executing the drill plan autonomously, it is anticipated that the accuracy, efficiency, and safety of the drilling operation will be enhanced. For AMV, the development of this control system will represent a significant technological step toward the objective of a fully autonomous drill jumbo.

1.2 The current state-of-the-art

While several major manufacturers worldwide produce drill jumbos, and although the industry trend is toward increased robotization, the control algorithms in these commercial solutions are typically proprietary and not publicly disclosed.

⋆ This work was financially supported by the Research Council of Norway (Norges forskningsråd) through the industrial PhD scheme (354230 - Autonomous Drilling Rig) and the SkatteFUNN R&D tax incentive scheme (90000440 - NextGen Drilling Rig).

Fig. 1. AMV drill jumbo with one articulated arm.

Autonomous drilling has received increasing attention also in the research community in recent years, and several studies have focused on developing forward and inverse kinematics algorithms for drill jumbos. Some of these also include automatic control sequences and provide simulation results. Forward kinematics solutions based on either Denavit-Hartenberg or screw-theoretic formulations have been proposed for different drill-rig configurations; Wang et al. (2014) extend the work of Jiang and Ahmed (2014) and investigate a forward kinematics approach using successive screw displacements. They also present an analytical inverse kinematics solution and an automatic drilling procedure, supported by simulation results. Cui et al. (2025) and Ho and Jianchi (1986) use the Denavit-Hartenberg convention for forward kinematics and also provide analytical inverse kinematics solutions. In contrast, Fink et al. (1996) describe a Cartesian control system for a redundant twin-boom rig, based on velocity kinematics and discuss manual and automatic control, but do not present either simulation or experimental results. Despite these efforts, existing research thus presents two significant limitations: 1) Most prior work relies on analytical inverse kinematics, which may be challenging to extend to manipulators with complex geometries, or hydraulic actuation characteristics. The AMV 7-DOF drill arm is both geometrically complex and hydraulically actuated. 2) The literature lacks full-scale validation of automatic drilling systems, with the majority of studies evaluated through simulations rather than real-world experiments.

This article investigates two algorithms that are suitable for complex manipulator geometries; the Product-of-Exponentials (PoE) forward kinematics method and the numerical Newton-Raphson inverse kinematics method. These algorithms are applied here to the AMV drill jumbo, but can also be readily adapted for other machines. The PoE method is similar to the successive screw displacements technique used by Wang et al. (2014). Notably, to the authors' knowledge, a numerical inverse kinematics solver has not previously been applied to drill jumbos. In addition, this work introduces an automatic control algorithm, validated by full-scale testing. The algorithm is related to the procedure in Wang et al. (2014). However, the algorithm presented in this work is more detailed and differs in that the seventh (feeder telescope) joint is excluded from the trajectory generation and is instead controlled separately. To the authors' knowledge, no previous research has presented full-scale testing of an automatic control algorithm based on numerical inverse kinematics.

In summary, this article makes the following contributions:

- **Numerical inverse kinematics for drill jumbos:** A Newton–Raphson inverse kinematics solver is applied to the AMV drill jumbo.
- **Automatic control algorithm with joint-level separation:** An automatic control algorithm integrating numerical IK, trajectory generation, and hydraulic PID control is developed. The seventh (feeder telescope) joint is treated separately from the trajectory generation to account for the specific requirements of the drilling process, resulting in a more detailed and practically applicable control structure than in prior work such as Wang et al. (2014).
- **First full-scale experimental validation of numerical IK–based autonomous drilling:** The proposed control system is validated in full-scale tests in Flekkefjord, Norway and in the Trælen mine, Norway. To the authors' knowledge, no previous research has reported full-scale testing of an automatic drilling system based on a numerical inverse kinematics solver.

2. THE AMV DRILL JUMBO

The drill jumbo manufactured by AMV is shown in Figure 1. The chassis integrates an operator cabin and one articulated arm. The drilling arm assembly, seen in Figure 2, is composed of two main parts, the boom and the feeder. The 7-DOF manipulator is actuated through the seven joints listed in Table 1, where the joint index, name, type, axis of rotation/translation, corresponding coordinate frame and symbol are given.

Table 1. Manipulator joints.

Joint	Name	Type	Axis	Frame	Symbol
1	Boom slew	Revolute	z	$\mathcal{F}_{bs}$	θ_1
2	Boom lift	Revolute	y	$\mathcal{F}_{bl}$	θ_2
3	Boom telescope	Prismatic	x	$\mathcal{F}_{bt}$	θ_3
4	Feeder rotation	Revolute	x	$\mathcal{F}_{fr}$	θ_4
5	Feeder lift	Revolute	y	$\mathcal{F}_{fl}$	θ_5
6	Feeder slew	Revolute	z	$\mathcal{F}_{fs}$	θ_6
7	Feeder telescope	Prismatic	x	$\mathcal{F}_{ft}$	θ_7

Figure 2 illustrates the home configuration of the manipulator. The positive directions of the x-, y-, and z-axes are defined as forward, leftward, and upward, respectively.

The kinematic structure of the manipulator is defined as the serial kinematic chain from the boom slew joint to the feeder slew joint. The feeder telescope joint is mainly used to establish contact with the face prior to drilling. Consequently, this joint is excluded from the 6-DOF model investigated for the inverse kinematics.

3. FORWARD KINEMATICS

For the AMV drill jumbo the space frame $\mathcal{F}_s$ is located at the ground, between the stabilizer legs, and represents the fixed world frame. For the 6-DOF manipulator, the body frame $\mathcal{F}_b$ coincides with the end-effector; the feeder slew frame $\mathcal{F}_{fs}$.

The forward kinematics determine the pose of the end-effector by utilizing the joint measurements and the geometry of the manipulator. Both the Denavit-Hartenberg convention (Spong et al., 2006) and the Product-of-Exponentials (PoE) approach (Lynch and Park, 2017) were considered for the forward kinematics problem. The

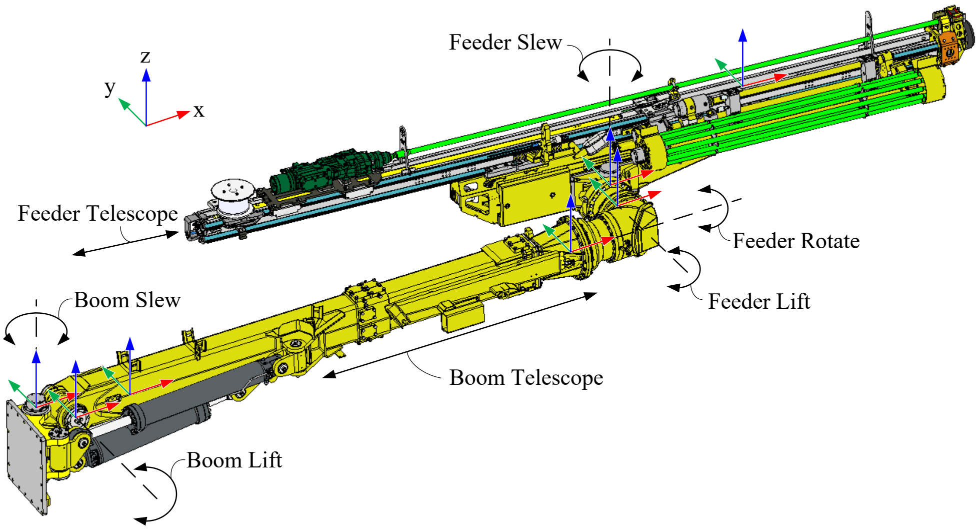

Fig. 2. Zeta X design. The manipulator consists of the boom and the feeder.

PoE method was deployed, due to its advantages when modeling complex manipulator geometries. As presented by Lynch and Park (2017), the Product-of-Exponentials formula for an n-joint serial manipulator is expressed as:

$$T(\theta) = e^{[\mathcal{S}_1]\theta_1} e^{[\mathcal{S}_2]\theta_2} \cdots e^{[\mathcal{S}_n]\theta_n} M. \tag{1}$$

Here, $T(\theta) \in SE(3)$ is the end-effector configuration, $M \in SE(3)$ is the home configuration, and $\mathcal{S}_i \in \mathbb{R}^6$ and $\theta_i \in \mathbb{R}$ correspond to the i-th screw axis and joint variable, respectively, expressed in the space frame $\mathcal{F}_s$.

The matrix exponential $e^{[\mathcal{S}_i]\theta_i}$, the screw axes $\mathcal{S}_i$, and the home configuration M in (1) are computed according to Lynch and Park (2017). The screw axes and home configuration are shown in Appendix A.

4. INVERSE KINEMATICS

An inverse kinematics solver computes the joint target configuration θ_t, required to align the end-effector with a target pose $T_{\text{hole}} \in SE(3)$. For the 6-DOF manipulator, this problem is solved by utilizing an iterative Newton-Raphson algorithm, following Lynch and Park (2017).

The target pose T_{hole} is computed based on the entry (x_1, y_1, z_1) and end (x_2, y_2, z_2) coordinates of the current drill hole, provided by the drill plan.

The Newton-Raphson method is fed with an initial joint guess $\theta_0 \in \mathbb{R}^6$, and subsequently improves this estimate to minimize the error between the current end-effector pose $T(\theta_i)$, and the target pose T_{hole}. The error is expressed as the spatial twist

$$\mathcal{V}_s = \begin{bmatrix} \omega_s \\ v_s \end{bmatrix}, \tag{2}$$

required to move the manipulator from $T(\theta_i)$ to the constant T_{hole}. The twist $\mathcal{V}_s \in \mathbb{R}^6$, and twist components $\omega_s \in \mathbb{R}^3$ and $v_s \in \mathbb{R}^3$ are expressed in the space frame $\mathcal{F}_s$. The algorithm terminates when the twist components ω_s and v_s are bounded by predefined tolerances:

$$||\omega_s|| < \epsilon_\omega, \tag{3}$$

$$||v_s|| < \epsilon_v. \tag{4}$$

The iterative Newton-Raphson algorithm is written as

$$\theta_{i+1} = \theta_i + J_s^{-1}(\theta_i)\mathcal{V}_s, \tag{5}$$

where $\theta_i \in \mathbb{R}^6$ and $\theta_{i+1} \in \mathbb{R}^6$ are the joint configuration at the current and next iteration, respectively. $J_s^{-1}(\theta_i) \in \mathbb{R}^{6x6}$ is the inverse Jacobian matrix expressed in the space frame $\mathcal{F}_s$.

4.1 Calculation of the spatial twist $\mathcal{V}_s$

For every iteration i, the pose error is calculated as

$$T_{\text{error}}(\theta_i) = T^{-1}(\theta_i) T_{\text{hole}}, \tag{6}$$

where the end-effector pose for the current joint configuration $T(\theta_i)$ is calculated based on (1).

To compute the 4×4 matrix representation of the body twist $[\mathcal{V}_b]$, the matrix logarithm algorithm is applied to the pose error:

$$[\mathcal{V}_b] = \log(T_{\text{error}}(\theta_i)). \tag{7}$$

The body twist

$$\mathcal{V}_b = \begin{bmatrix} \omega_b \\ v_b \end{bmatrix} \tag{8}$$

components are obtained from $[\mathcal{V}_b]$ as

$$[\mathcal{V}_b] = \begin{bmatrix} [\omega_b] & v_b \\ 0 & 0 \end{bmatrix}, \tag{9}$$

where $[\omega_b]$ is the skew-symmetric matrix representation of ω_b.

Since the iterative Newton-Raphson algorithm in (5) is defined in the space frame, the body twist must be transformed to the space twist. This transformation is accomplished by using the adjoint matrix representation of the end-effector configuration $T(\theta_i)$. The space twist $\mathcal{V}_s$ is calculated as

$$\mathcal{V}_s = [\text{Ad}(T(\theta_i))]\mathcal{V}_b. \tag{10}$$

For an arbitrary 4×4 homogeneous transformation

$$T = \begin{bmatrix} R & p \\ 0 & 1 \end{bmatrix}, \tag{11}$$

the corresponding 6×6 adjoint matrix representation is calculated as

$$\mathrm{Ad}_T = \begin{bmatrix} R & 0 \\ [p]R & R \end{bmatrix}, \tag{12}$$

where $[p]$ is the skew-symmetric representation of p.

4.2 Calculation of the space Jacobian $J_s(\theta^i)$

The space Jacobian $J_s(\theta) \in \mathbb{R}^{6\times6}$, defines the relationship between the joint rate vector $\dot{\theta} \in \mathbb{R}^6$ and the spatial twist $\mathcal{V}_s \in \mathbb{R}^6$ of the end-effector expressed in the space frame $\mathcal{F}_s$. Hence, the spatial twist is calculated as:

$$\mathcal{V}_s = J_s(\theta)\dot{\theta}. \tag{13}$$

The Jacobian is constructed column-wise

$$J_s(\theta) = [J_{s1}(\theta)\ J_{s2}(\theta)\ ...\ J_{s6}(\theta)], \tag{14}$$

where each column $J_{si}(\theta)$ is computed based on the i-th joint screw axis $\mathcal{S}_i$.

The first column corresponds to the first screw axis, $J_{s1} = \mathcal{S}_1$. The subsequent columns $J_{s2}(\theta)...J_{s6}(\theta)$ are computed by transforming the i-th joint screw axis $\mathcal{S}_i$ according to the motion of the preceding $i-1$ joints. This transformation is calculated by using the adjoint representation of the accumulated homogeneous transformations:

$$J_{si}(\theta) = \mathrm{Ad}_{e^{[\mathcal{S}_1]\theta_1}\cdots e^{[\mathcal{S}_{i-1}]\theta_{i-1}}}(\mathcal{S}_i). \tag{15}$$

4.3 Calculation of the inverse space Jacobian $J_s^{-1}(\theta)$

For the 6-DOF manipulator, the space Jacobian $J_s(\theta)$ is a 6×6 square matrix. The manipulator is neither redundant nor underactuated since the number of joints ($n = 6$) corresponds to the dimension of the task space.

The manipulator may still experience singularities. This occurs when the space Jacobian loses full rank, i.e. $\det(J_s(\theta)) = 0$. Near singularities, the inverse may be undefined or numerically unstable, leading to large joint velocities.

In order to ensure robust manipulator behavior for the entire workspace, including close to singular configurations, the inverse space Jacobian is computed by utilizing the damped least squares method. This is also known as the Levenberg-Marquardt method and computes the pseudo-inverse of the space Jacobian $J_s^{-1}(\theta)$ as follows:

$$J_s^{-1}(\theta) = J_s^{\top}(\theta)(J_s(\theta)J_s^{\top}(\theta) + \lambda^2 I)^{-1}. \tag{16}$$

Here, $J_s^{\top}(\theta)$ is the transpose of the space Jacobian, λ is a non-zero damping factor and I is the 6×6 identity matrix.

5. AUTOMATIC CONTROL

Automatic control is realized by implementing Algorithm 1 in the robotic control system. The algorithm is designed to enable the manipulator to execute the entire drill plan, drilling every blast hole until all holes have been visited.

5.1 Trajectory generation

ROS2's (Robot Operating System 2) path planning and trajectory generation algorithms were used to compute the joint position and velocity trajectories, $\theta_d(t)$ and $\dot{\theta}_d(t)$, respectively, enabling the manipulator to move from the current hole to the next (Macenski et al., 2022). In particular, the manipulator library MoveIt2, which is part of ROS2's infrastructure, offers multiple algorithms for kinematics, path planning, and trajectory generation (Coleman et al., 2014).

Algorithm 1 Automatic Control

```
while hole index i_hole ≠ number of holes n_holes do
    while the current feeder telescope position θ_{c,7} is
            above the feeder telescope retract setpoint
            θ_{d,7} do
        Retract the feeder telescope.
    end while
    Request the next target hole pose T_hole.
    Use the Newton-Raphson algorithm in (5) to
     compute the target joint configuration θ_t for the hole
     pose T_hole.
    Generate joint position and joint velocity
     trajectories, θ_d(t) and θ̇_d(t), respectively, from the
     current joint configuration θ_c to the target joint
     configuration θ_t.
    Initialize timer t and joint tolerances θ_tol.
    while θ_tol < abs(θ_t − θ_c) do
        Compute the time duration Δt from the previous
         execution.
        Update timer t = t + Δt.
        Sample θ_d(t) and θ̇_d(t).
        Feed the obtained joint position and joint
         velocity setpoints, θ_d and θ̇_d, respectively, to the
         PID controllers.
    end while
    while the drill bit is not contacting the face do
        Extend the feeder telescope.
    end while
    Initiate the rock drill. Activate percussion and
     rotation.
    while the drill bit is not at the target hole depth do
        Extend the rock drill along the feeder, move the
         drill string into the rock.
    end while
    while the rock drill is not at its start position do
        Retract the rock drill.
    end while
    i_hole = i_hole + 1
end while
```

The trajectory generation was performed in two stages. First, the MoveIt2 Pilz industrial motion planner pipeline generated a feasible kinematic path from the current joint configuration θ_c to the target pose T_{hole}. A predefined workspace constrained the path generation. Next, the MoveIt2 time-optimal trajectory generation algorithm time-parameterized the kinematic path, yielding time-optimal joint position $\theta_d(t)$ and joint velocity trajectories $\dot{\theta}_d(t)$ for the 6-DOF manipulator.

5.2 Controllers

Hydraulic cylinders and motors actuate the joints of the 7-DOF manipulator. Changes in hydraulic flow and pressure induce motion. This is achieved by controlling their corresponding compensated proportional valves. These valves are bidirectional, a fully open valve (100%) induces maximum positive joint velocity, and a fully closed valve (0%) results in zero velocity. The control signal applied to each valve is constrained within the range [-10000, 10000], corresponding to [-100%, 100%].

The control law

$$u_j(t) = k_{p,j}e_j(t) + k_{i,j}\int_0^t e_j(\tau)d\tau + k_{d,j}\frac{d}{dt}e_j(t) + k_{ff,j}\dot{\theta}_{d,j}(t), \tag{17}$$

is applied to the proportional valve of each joint j. $k_{p,j}$, $k_{i,j}$, $k_{d,j}$, and $k_{ff,j}$ are the proportional, integral, derivative, and feedforward controller gains, respectively. $\dot{\theta}_{d,j}(t)$ is the desired joint velocity at time t from Algorithm 1. The position error $e_j(t)$ is the deviation between the desired and current joint position at time t and is computed as:

$$e_j(t) = \theta_{d,j}(t) - \theta_{c,j}(t). \tag{18}$$

$\theta_{d,j}(t)$ is the desired joint position at time t provided by Algorithm 1, while $\theta_{c,j}(t)$ is the measured joint position at time t.

6. EXPERIMENTAL RESULTS

The accuracy of the robotic control system was tested experimentally at AMV's test facilities in Flekkefjord, Norway, and in the Trælen mine, Norway. For both full-scale field experiments, the robotic control system was provided with a digital drill plan comprising multiple drill holes with position and orientation.

Fig. 3. Test setup in the Trælen mine.

To localize the drill jumbo relative to the rock face, three retroreflective targets were mounted on the left-hand side of the chassis and on the face. The positions of the targets were identified using a stationary RIEGL VZ-400i LiDAR scanner, illustrated in Figure 3. These coordinates were then entered into the robotic control system, which utilized them to convert the drill holes to local drill jumbo coordinates in the space frame $\mathcal{F}_s$.

Following the setup described above, the drill plans in Table 2 and 3 were executed using Algorithm 1. In these tables, i denotes the hole index, and (x_1, y_1, z_1) and (x_2, y_2, z_2) represent the entry and end coordinates of the holes, respectively.

Table 2. Drill plan for the Flekkefjord experimental campaign [m].

i	x_1	y_1	z_1	x_2	y_2	z_2
1	10.659	0.675	2.218	14.659	0.675	2.218
2	10.390	1.592	1.419	14.390	1.592	1.419
3	10.399	2.550	2.565	14.399	2.550	2.565
4	10.100	3.861	1.529	14.100	3.861	1.529

Table 3. Drill plan for the Trælen mine experimental campaign [m].

i	x_1	y_1	z_1	x_2	y_2	z_2
1	10.695	1.963	3.158	15.776	2.251	3.423
2	11.271	2.019	2.388	15.775	2.274	2.623
3	10.934	2.024	1.571	15.773	2.298	1.823
4	11.002	2.051	0.775	15.772	2.321	1.024
5	11.188	1.018	0.756	15.730	0.879	0.982
6	11.214	0.217	0.735	15.706	0.080	0.959
7	11.144	-2.181	0.666	15.636	-2.318	0.889

The drilled holes for the Trælen mine experiments are shown in Table 4. Here, (x, y, z) denotes the drilled holes entry point coordinates, which were determined by the LiDAR scanner. (dx, dy, dz) is the difference between the planned and drilled holes entry point coordinates, (x_1, y_1, z_1) and (x, y, z), respectively.

Table 4. Drilled holes for the Trælen mine experimental campaign [m].

i	x	y	z	dx	dy	dz
1	10.635	1.952	3.202	0.060	0.012	-0.044
2	10.985	2.020	2.478	0.286	0.000	-0.090
3	10.881	2.135	1.578	0.053	-0.112	-0.007
4	10.913	2.304	0.793	0.089	-0.253	-0.018
5	11.283	1.176	0.789	-0.096	-0.158	-0.033
6	11.301	0.369	0.812	-0.087	-0.152	-0.077
7	11.246	-2.026	0.706	-0.102	-0.155	-0.040

For the Trælen mine experiments, the drilled hole position deviation, e, was calculated as:

$$e = \sqrt{dx^2 + dy^2 + dz^2}. \tag{19}$$

For the Flekkefjord experiments, these deviations were determined by measuring the Euclidean distance between the centers of each planned hole and its corresponding drilled hole. Table 5 shows that the mean position deviations for the Flekkefjord and Trælen mine experimental campaigns were 4.6 cm and 19.1 cm, respectively.

Table 5. Position deviation e per drill hole for both experimental campaigns [m].

i	Flekkefjord	Trælen mine
1	0.020	0.076
2	0.080	0.300
3	0.005	0.124
4	0.080	0.269
5	–	0.188
6	–	0.191
7	–	0.190
Mean	0.046	0.191

During these two campaigns, the rock face varied significantly in smoothness at the drill hole locations. Specifically, at the Trælen mine, the feeder slid sideways upon contact with the rock face, resulting in greater drill hole deviation than in the Flekkefjord campaign, where the rock face was smoother. To address this, the feeder extension control in Algorithm 1 should be less aggressive, and the rock face should be analyzed before drilling.

7. CONCLUSION AND FUTURE WORK

A robotic control system has been developed and deployed for the AMV drill jumbo with one articulated arm. The system implements a complete automatic drilling algorithm that integrates Product-of-Exponentials forward kinematics, a Newton–Raphson numerical inverse kinematics solver, trajectory generation using ROS2/MoveIt2, and PID control of the hydraulic joints. The final feeder telescope joint is handled separately to establish contact with the rock face and to perform the drilling motion along the feeder.

The proposed control system autonomously executed digital drill plans in full-scale experimental campaigns in Flekkefjord, Norway and the Trælen mine, Norway. To the authors' knowledge, this constitutes the first full-scale experimental demonstrations of numerical inverse-kinematics–based autonomous drilling on an industrial drill jumbo. The system achieved an average drilled-hole accuracy of 4.6 cm and 19.1 cm in the Flekkefjord and Trælen mine experimental campaigns, respectively. The former level of accuracy is acceptable for many holes in a typical drill plan, but is insufficient for holes near the tunnel floor and periphery, where tighter tolerances are required to prevent overbreak. The latter level of accuracy is not acceptable for any holes in the drill plan. Hence, to autonomously drill the entire drill plan, further improvements are necessary. Future work will thus focus on increasing the drilling accuracy of the robotic control system.

ACKNOWLEDGEMENTS

This work was supported by the DINAMINE project, which is funded by the Horizon Europe research and innovation programme (Grant Agreement No. 101091541). Views and opinions expressed are however those of the authors only and do not necessarily reflect those of the European Union or the European Health and Digital Executive Agency (HaDEA). Neither the European Union nor the granting authority can be held responsible for them.

DECLARATION OF GENERATIVE AI AND AI-ASSISTED TECHNOLOGIES IN THE WRITING PROCESS

During the preparation of this work, the author used ChatGPT 5.0, Google Gemini 2.5 Pro, and Grammarly Pro to identify grammatical errors and ensure better text flow. The former two were also used to supplement the literature search, providing suggestions for research articles relevant to the work in this paper. After using these tools, the author reviewed and edited the content as needed and takes full responsibility for the content of the publication.

REFERENCES

Coleman, D., Şucan, I., Chitta, S., and Correll, N. (2014). Reducing the barrier to entry of complex robotic software: a moveit! case study. *J. of Software Engineering for Robotics*, 5(1), 3–16.

Cui, Y., Liu, S., Shu, Z., Lv, Z., and Li, L. (2025). Positioning error prediction and compensation for the multi-boom working mechanism of a drilling jumbo. *J. of Zhejiang University-SCIENCE A*, 26(1), 66–77.

Fink, B., Hiller, M., Krolls, H., and Schweikart, S. (1996). Concepts of an advanced cartesian control system for a redundant twin boom drill rig. In *Proc. of the 13th ISARC*, 103–112. IAARC, Tokyo, Japan.

Ho, C.Y. and Jianchi, Y. (1986). Design of automated jumbo drilling robot manipulator. In *IFAC Automation in Mining, Mineral and Metal Processing*, 59–66. IFAC, Tokyo, Japan.

Jiang, Q. and Ahmed, S.N. (2014). The Kinematics of 6R-2P Mining Drill Jumbo. *J. of Mechanisms and Robotics*, 6(3), 034501–1–4.

Li, Y., Peng, P., Li, H., Xie, J., Liu, L., and Xiao, J. (2023). Drilling Path Planning of Rock-Drilling Jumbo Using a Vehicle-Mounted 3D Scanner. *Sustainability*, 15(12).

Lynch, K.M. and Park, F.C. (2017). *Modern Robotics: Mechanics, Planning, and Control*. Cambridge University Press, Cambridge, UK.

Macenski, S., Lalancette, C., Foote, T., Gerkey, B., and Woodall, W. (2022). Robot operating system 2: Design, architecture, and uses in the wild. *Science Robotics*, 7(66), eabm6074.

Mancini, R., Badino, V., Innaurato, N., Fornaro, M., Cardu, M., Baldo, G.L., and Borla, G. (1996). Technical and Economic Aspects of Tunnel Blasting Accuracy Control. *Tunnelling and Underground Space Technology*, 11(4), 455–463.

Spong, M.W., Hutchinson, S., and Vidyasagar, M. (2006). *Robot Modeling and Control*. John Wiley & Sons, Hoboken, NJ.

Wagner, H. (2019). Deep Mining: A Rock Engineering Challenge. *Rock Mechanics and Rock Engineering*, 52, 1417–1446.

Wang, Y., Fang, C., Jiang, Q., and Ahmed, S.N. (2014). The Automatic Drilling System of 6R-2P Mining Drill Jumbos. *Advances in Mechanical Engineering*, 7(2).

Appendix A. MATRICES

$$M = \begin{bmatrix} 1 & 0 & 0 & 5.63 \\ 0 & 1 & 0 & 0.82 \\ 0 & 0 & 1 & 2.28 \\ 0 & 0 & 0 & 1 \end{bmatrix} \tag{A.1}$$

$$\mathcal{S}_1 = [0.0\ 0.0\ 1.0\ 0.198\ -0.110\ 0.0]^T \tag{A.2}$$

$$\mathcal{S}_2 = [0.0\ 1.0\ 0.0\ -2.162\ 0.0\ 0.281]^T \tag{A.3}$$

$$\mathcal{S}_3 = [0.0\ 0.0\ 0.0\ 1.0\ 0.0\ 0.0]^T \tag{A.4}$$

$$\mathcal{S}_4 = [1.0\ 0.0\ 0.0\ 0.0\ 2.182\ -0.197]^T \tag{A.5}$$

$$\mathcal{S}_5 = [0.0\ 1.0\ 0.0\ -2.182\ 0.0\ 5.529]^T \tag{A.6}$$

$$\mathcal{S}_6 = [0.0\ 0.0\ 1.0\ 0.823\ -5.629\ 0.0]^T \tag{A.7}$$